Shape-based features of white matter fiber-tracts associated with outcome in Major Depression Disorder

Claire Cury, Jean-Marie Batail, Julie Coloigner

Shape-based features of white matter fiber-tracts associated with outcome in Major Depression Disorder

Claire Cury[1], Jean-Marie Batail[2], and Julie Coloigner[1]

[1] Univ Rennes, CNRS, Inria, Inserm, IRISA UMR 6074, Empenn ERL U-1228, F-35000 Rennes, France
[2] Centre Hospitalier Guillaume Régnier, Academic Psychiatry Department, 35703 Rennes, France

Abstract. Major depression is a leading cause of disability due to its trend to recurrence and treatment resistance. Currently, there are no biomarkers which could potentially identify patients with risk of treatment resistance. In this original paper, we propose a two-level shape analysis of the white matter bundles based on the Large Diffeomorphic Deformation Metric Mapping framework, to study treatment resistant depression. Fiber bundles are characterised via the deformation of their center line from a centroid shape. We developed two statistical analyses at a global and a local level to identify the most relevant bundles related to treatment resistant depression. Using a prospective longitudinal cohort including 63 patients. We applied this approach at baseline on 50 white matter fiber-tracts, to predict the clinical improvement at 6 months. Our results show a strong association between three bundles and the clinical improvement 6 months after. More precisely, the right-sided thalamo-occipital fascicle and optic radiations are the most robust followed by the splenium. The present study shows the interest in considering white matter shape in the context of depression, contributing to improve our understanding of neurobiological process of treatment resistance depression.

Keywords: Computational Anatomy · Depression · Fibre bundles.

1 Introduction

Depression is a worldwide leading cause of disability due to its trend to recurrence and treatment resistance [15,10]. The Sequenced Treatment Alternatives to Relieve Depression (STAR*D) trial has indeed demonstrated that 30% of patients remained depressed after 4 trials of antidepressants (ATD) [21]. The remission rate dropped dramatically after the second ATD trial. The last two decades have been marked by an increasing interest in research on biomarkers that could help to identify at risk patients of Treatment Resistant Depression (TRD) and to guide in the therapeutic strategies [16,28].

Advances in neuroimaging have improved our understanding of the neural circuit involved in depression. The structural connectivity from diffusion-weighted

Magnetic Resonance Imaging (dMRI) has provided valuable insights on the white matter abnormalities associated with depression and different depressive phenotypes [4]. Therefore, to date, there is no consensual imaging biomarkers of TRD which could potentially improve our understanding the pathophysiology of this poor outcome [8]. Only few studies examined the relation between neuroimaging information and TRD [1]. Thus, cross-sectional works have emphasized that white matter abnormalities affecting networks related to emotion regulation such as cortico-subcortical circuits as well as subgenual anterior cingulate cortex are involved in the TRD pathophysiology [23]. However, these studies have reported only moderate correlations between TRD and white matter microstructure metrics derived from dMRI. While the large majority of dMRI studies in depression focuses on voxel-based analysis of microstructure metrics, we propose a shape-based analysis of white matter fiber-tracts. The shape variability of those bundles (3D curves) may yield new insights into normal and pathologic brain development [11,12].

In this original paper, we propose a two levels shape analysis of the white matter bundles using the Large Diffeomorphic Deformation Metric Mapping framework (LDDMM), now well-known in computational anatomy, that has the great advantage to embed shapes into a Riemannian manifold. In LDDMM Shapes can be characterised via the deformations of their center line to a centroid shape. Our original approach is to analyse those deformations by estimating local and global features, used to model the association between white matter fiber bundles and TRD. The goal is to address the question : is there baseline shape-based biomarkers on white matter tracts able to predict the outcome of a depressed patient 6 months after? Using a prospective longitudinal cohort, we applied this approach at baseline on 50 white matter fiber-tracts, to predict the clinical improvement at 6 months.

2 Data and pre-processings

Population and Imaging acquisition : Sixty-three depressed patients were recruited from routine care units in the psychiatric university hospital of Rennes. They were enrolled in a prospective longitudinal cohort study, which was approved by an ethic committee and registered in www.clinicaltrial.gov (NCT 02286024). Written informed consents were obtained from all subjects. Depressed patients underwent clinical interview and examination including routine neuropsychological testing at baseline and 6 months after. The Clinical Global Impression – improvement scale (CGI-I) was used at 6-months to measure the treatment response [13]. This measure is a well-established rating tool applicable to all psychiatric disorders and well correlated with other standard scales [2]. It provides a global rating of illness severity and improvement, taking into accounts the patient's history, social circumstances, symptoms and the impact of the illness on the patient's ability to function : The CGI-I measure is rated from 1 (very much improved) to 7 (very much worse) [2]. A demographic table is given in supplementary material. At baseline, patients were scanned on a 3T

Verio Siemens MR scanner with a 32-channel head coil. The 3D T1-weighted image was acquired covering the whole brain (176 sagittal slices) with TR = 1.9 s, TE = 2.26 ms, flip angle = 9°, resolution = 1 mm× 1 mm× 1 mm, FOV = 256 mm ×256 mm). The dMRI data were gathered on 60 slices using an interleaved slice acquisition, no gap, resolution= 2 mm×2 mm×2 mm and in a 256 mm ×256 mm field of view. The acquisition and reconstruction matrices were 128 × 128, using 30 directions and a b-value of 1000 s/mm^2. TR/TE = 11,000/99 ms, flip angle was 90° and pixel bandwidth was 1698 Hz.

Diffusion image processing: Diffusion images were corrected, using the open source Anima toolbox[3], for eddy current-induced image distortion using a block-matching distortion correction method ensuring an opposite symmetric transformation [14]. Then, the individual B0 image was co-registered with the structural image with 1 mm isotropic resolution, using a linear block-matching algorithm [19,5]. For EPI distortion correction, the B0 image was non-linearly registered to the structural image with a linear block-matching algorithm [5]. A rigid realignment was performed between the 30 dMRIs to compensate for subject motion. Then, denoising step using blockwise non-local means filtering was applied [6]. Skull stripping was also performed using the Anima toolbox. Diffusion images were transformed into the Montreal Neurological Institute (MNI) template space, in two steps : The structural image was non-linearly transformed to the MNI template space, using block-matching algorithms [19,5]; Then, we applied those transformations to the pre-processed diffusion images to transform them into the MNI space.

Center line estimation : Single-shell single-tissue constrained spherical deconvolution was used to extract the fibre orientation distributions [24] and then anatomically constrained probabilistic tractography was performed using MRtrix toolbox [25] to estimate the white matter bundles. Then, the automated pipeline TractSeg was used to generate 50 bundle-specific tractograms [29]. This tool is based on convolutional neural networks trained to create tract orientation maps, enabling the creation of accurate bundle-specific tractograms. For each bundle, a center line was determined using QuickBundles [9]. A distance measure called minimum average direct flip was used to calculate the center line of 100 points, for each bundle of each patient.

3 Proposed methodology

3.1 Shape representation and framework

To analyse the center lines we used the deformation-based Large Diffeomorphic Deformation Metric Mapping (LDDMM) framework, that generates a time-dependent flow of diffeomorphisms between two shapes [26]. In the LDDMM framework, the shortest diffeomorphism between two objects happens to be a geodesic, embedding them into a Riemannian manifold and allowing the analysis of shapes on the tangent space at a given point of the manifold.

[3] `https://github.com/Inria-Visages/Anima-Public/wiki`

In brief (for more details one can refer to [26,20]), and to introduce some notations, a deformation is defined by integrating time-varying velocity vector fields $v(t)$ (with time $t \in [0;1]$), belonging to the reproducing kernel Hilbert space V. This is the closed span of vectors fields of the form $K_V(x,\cdot)\alpha$ with K_V a kernel and $\alpha_m(t) \in \mathbb{R}^3$ a time-dependent vector called momentum vector defined at point x_m and time t. The optimal deformation Φ between the shape of bundle i of subject j_1 (i.e. a centre line) and subject j_2 is estimated by minimising the functional $J(\Phi) = \gamma Reg(v(t)) + \|\Phi(B_{i,j_1}) - B_{i,j_2}\|_2^2$, where γ weights the regularisation and the data fidelity terms, and $Reg(v(t))$ is the energy enforcing $v(t)$ to stay in the space V. Here, we selected the sum of squared distance for the fidelity data term, since center lines (one smooth line per subject) can be considered as a set of landmarks. This choice also speed up computation time and avoid extra parameter tuning. Here, the optimal deformation Φ is a geodesic from B_{i,j_1} to B_{i,j_2} and is then fully encoded by the set of initial momentum vectors $\boldsymbol{\alpha}^{j_2}_{B_{i,j_1}}(0) = \{\alpha^{j_2}_m(0)\}_{m\in\{1,...,M\}}$ defined at landmark positions x_m of shape $B_{i,j_1} = \{x_m\}_{m\in\{1,...,M\}}$. The initial momentum vectors allow to analyse deformations on the tangent space at a given position, then we analyse a population of shape through their deformations from a centroid point on the manifold.

3.2 Shape features extraction

For a given bundle i and for each subjects j, the features we are interested in this paper are the set of initial momentum vectors $\{\boldsymbol{\alpha}^j_{B_i}(0)\}_j$ going from a centroid point (B_i) on the manifold of the i-th bundle towards subjects j. To do so, we first estimate this centroid shape of the i-th bundle $B_i = \{x_m\}_{m\in\{1,...,M\}}$ as proposed in [7]. A centroid shape is computed by iteratively adding a new subject of the population at each step. This method only requires $N-1$ deformation estimations (i.e. minimisation of $J(\Phi)$). Then, we computed the deformations from the centroid shape of a bundle B_i to each subject's shape j to obtain the set of initial momentum vectors $\{\boldsymbol{\alpha}^j_{B_i}(0)\}_{j\in\{1,...,N\}} = \{\alpha^j_m(0)\}_{m\in\{1,...,M\}}, \forall j \in \{1,...,N\}$, for a total of $2N-1$ shape registrations. For each centroid bundle B_i, to analyse the corresponding $\{\boldsymbol{\alpha}^j_{B_i}(0)\}_j$ for all subjects j, we propose two types of features : local and global.

Local features describe initial momentum vectors at each landmark positions across all subjects. We define those local features of each initial momentum vectors, located at each point on the centroid shape B_i, as spherical coordinates using the average vector as the pole : amplitude, polar and azimuthal angles. The amplitude of $\{\alpha^j_m(0)\}$ captures the amount of deformation which is the distance to the centroid of the population. To capture vector orientations, we calculated, for each landmark x_m of the bundle i the polar angle between the vector $\alpha^j_m(0)$ and $v_1 = \sum_{j=1}^N \alpha^{i,j}_m(0)/N$, the average of initial momentum vectors of the population, and its azimuthal angle. To build an orthogonal vector v_3 to v_1, where $v_3 = v_1 \times v_2$, we arbitrarily choose a vector $v_2 = v_1 + (1,1,1)$ to preserve the connection between v_1 and v_2 across all x_m along a bundle i. The azimuth is the angle between $\alpha^j_m(0)$ and the vector v_3.

Global features are defined to capture global shape changes and therefore do not focus on momenta $\alpha_m^j(0)$ independently. Global features are estimated through a Kernel Principal Component Analysis (K-PCA) [22] on $\{\boldsymbol{\alpha}_{B_i}^j(0)\}_{j\in\{1,...,N\}}$ in the tangent space at the centroid shape B_i position. We used the same kernel K_V of the space of deformations. For the global analysis, we used the 5 first eigenvectors, explaining the most important deformations of each bundles.

3.3 Analysis

We defined two linear models, one using the global features (i.e. 5 principal components), and the other one including the local features (i.e. M amplitudes, and $2 \times M$ angular distances for the orientations), to assess the association between those features and the clinical improvement score 6 months after, called CGI-I. As co-factors in both models, we used for each patient : disease duration, age, gender, and the medication load including four types of drugs (anti-depressant, mood stabiliser, anti-psychotic, benzodiazepine).

To improve and challenge the robustness of the different models, especially for the local features, as they depend on the number and position of landmarks, we used 10 different numbers of landmarks with $M \in \{5, 6, 7, 8, 9, 10, 11, 13, 15, 20\}$. We did not add more landmarks to keep the computation times reasonable, and to avoid having a too high number of co-factors, since for the local model, the number of features depend on the number of landmarks. We also augmented the data, by adding to each subjects 4 noisy versions of each bundles, increasing the size of the dataset from 63 to 315. To do so, a Gaussian noise on each central line was added. The dataset augmentation and the use of different landmarks lead to more than 300000 minimisation of functional J for deformation estimations. Finally, to gain in robustness and minimise false discoveries, each of the $2 \times 10 \times 50$ models are estimated 63 times using a leave-one-out approach. The number 63 corresponds to the original number of patients used in this study. To avoid introducing bias, the leave-one-out is actually a leave-5-out, removing at each step a patient's bundle and its 4 noisy versions. To estimate comparable coefficients, we standardised all variables and co-factors, and to assess the performance of the model, we use the adjusted R^2 that represents the amount of the variation in CGI-I explained by variables and co-factors, adjusted for the number of terms in the model. From the leave-5-out approach, we derived mean and 95% confidence interval for adjusted R^2, for model p-values and for variables coefficients.

4 Results

Figure 1 shows all the observations used and the 50 centroid shapes, one per bundle, used as tangent location to estimate $\{\boldsymbol{\alpha}_{B_i}^j(0)\}_j$, $\forall i \in \{1, ..., 50\}$ and $j \in \{1, ..., 315\}$. For each bundle we have 10 local models and 10 global models. First, to identify bundles of interests, we consider a model to be a good candidate when 1/ the 95% confidence interval of the model's p-value is under the threshold

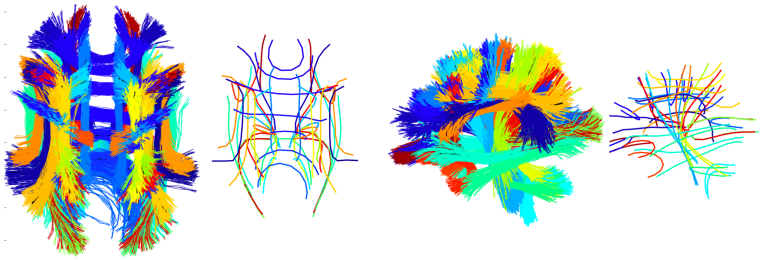

Fig. 1. Axial and sagittal views of all 50∗315 bundles center lines of the 315 observations (i.e. 63 patients and 4 noisy versions for each bundle) on the left side of each view and the corresponding 50 centroid shapes on the right side of each view.

5.10^{-5} (i.e. 0.05 corrected for multiple comparisons), 2/ the lower part of the 95% confidence interval of adjusted R^2 is higher than 0.3, meaning we consider only models that explain at least 30% of the variance. Then, we consider that a bundle has significant shape features, and is therefore of interest, when 3/ at least one of the approach (local or global) passes condition 1/ and 2/ for 10 out of 10 and the other approach for at least 5 out 10. Figure 2 displays, for each of the

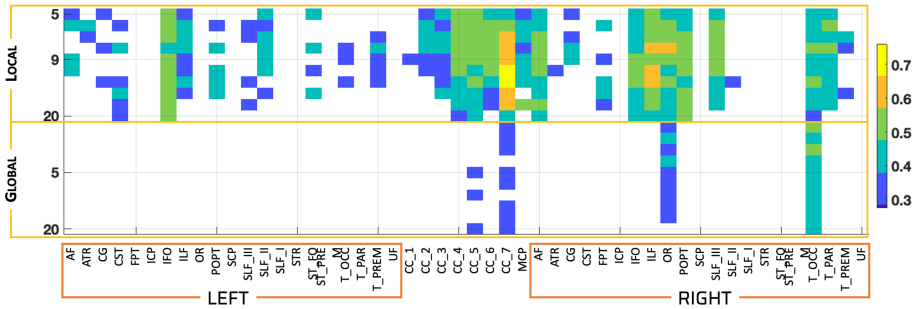

Fig. 2. The colorbar indicates the mean adjusted R^2 for models passing conditions 1/ and 2/. The y-axis indicates the number of landmark used for the 10 local model (on top) and the 10 global model (bottom).

10 models the adjusted R^2 value when passing conditions 1/ and 2/. The mean adjusted R^2 values ranges from 0.33 to 0.76. Bundles passing all 3 conditions are the splenium of the corpus callosum (CC7), the right optic radiation (OR) and the right thalamo-occipital fascicule (T-OCC). For all models passing conditions 1/ and 2/ (Figure 2), except two (local models, $M = 5$ for OR and T-OCC left), shape features contribution significantly to the model. There is no consistent bundles on the left hemisphere. The maximum adjusted R^2 value is obtained by the CC7 with a mean value of 0.76 (confidence interval $[0.74, 0.78]$). More details on statistics can be found in supplementary materials.

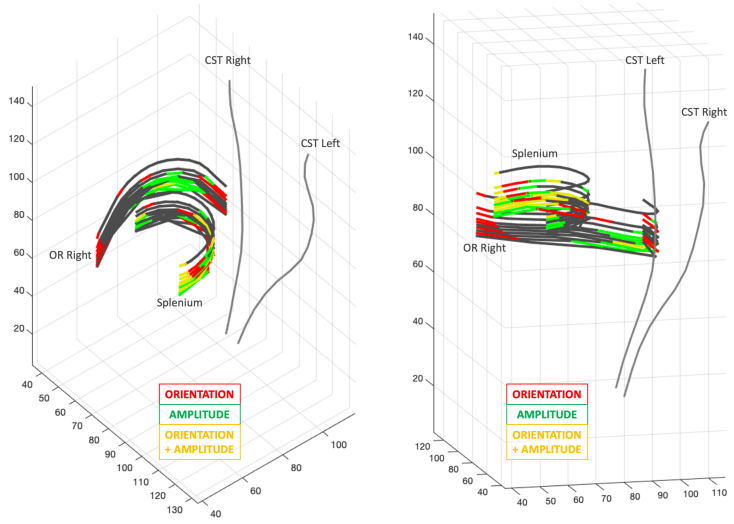

Fig. 3. The 10 different samplings of the right optic radiation (OR) and splenium of the corpus callosum, with significant landmarks indicated in red for orientation, green for amplitude, and yellow when both features are significant. Each centroid shape is shift in z-axis in function of the number of landmarks for display purposes. The cortico-spinal tract (CST) is used as a 3D referential.

For the local model, Figure 3 shows, for each sampling, landmarks with significant features involved in the model and the color depends on the type of feature : amplitude, orientation (polar or azimuth) or both. The T-OCC is not displayed in the figure as it is very close to the OR, therefore difficult to display together. The location along the T-OCC and OR centroid lines of significant features are consistent across samplings, furthermore the "corner" of the optic radiation seems to be where shape differences are associated to CGI-I.

For the global model, the right T-OCC is the only one to have 10 significant models. Principal Components (PC) 1, 4 and 5 are relevant to those 10 models, and PC 1 always has the strongest coefficient. From the principal eigenvectors E we computed the k-th principal mode of deformations $\mu^k = \overline{\boldsymbol{\alpha}(0)} + \sum_{j=1}^{N} E_j^k(\boldsymbol{\alpha^j}(0) - \overline{\boldsymbol{\alpha}(0)})$. We then can display the principal mode of variations μ^k by computing the exponential map of μ^k at B_i, for different times $t = -2$ to $t = 2$ along the geodesic. Figure 4 illustrates the 5 first principal modes of deformation of right T-OCC for 7, 10 and 15 landmarks. Each PC captures the same deformations, with a reduced explained variance when increasing the number of landmarks. This result is expected since different samplings do not affect the global shape of a center line, and increasing the sampling adds small information along the curve that reduces the explained variance.

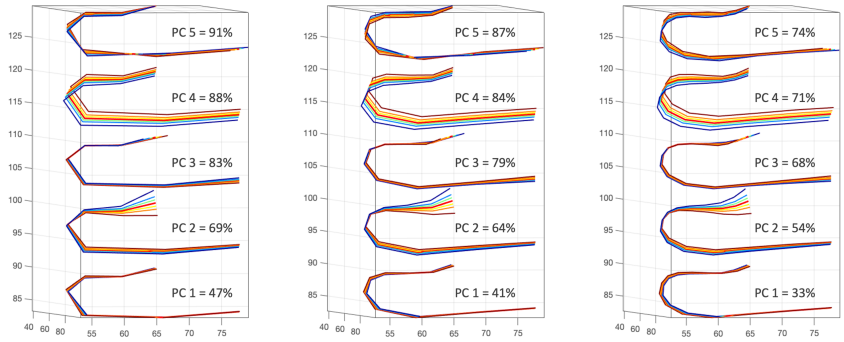

Fig. 4. Right T-OCC principal modes of deformations for 7, 10 and 15 landmarks (from left to right), with the corresponding cumulative explained variance.

5 Discussion and conclusion

In this paper, we analyse local and global shape features of 50 bundles in order to identify the bundles associated with poor outcome at 6 months in patients suffering from depression. First, our results show that right-sided T-OCC and OR are the most significant bundles, followed by CC7, associated with depression outcome at 6 months. These principal results are consistent with prior finding [17,4] where white matter micro-structures changes were observed in frontal-limbic circuits, such as T-OCC and CC7 (splenium), involved in the pathophysiological mechanisms of depression. Widespread abnormalities in MDD have been reported [27] specifically in CC7 which has been linked with anxiety [4]. Besides, abnormalities of cortico-subcortical projections (such as in OR oand T-OCC) are involved in cognitive and emotional regulation in depression [30,18]. Another study also highlighted the role of the thalamus in poor outcome in depression [1]. Moreover, our models show more coherence across sampling on the right hemisphere (Figure 2). Specifically, a recent study [3] showed a left-right asymmetry, where resistant patients had lower fractional anisotropy in right afferent fibers of the fronto-limbic circuit, and reduced connectivity between the regions connected to the right basal ganglia (i.e. involving thalamic connections), compared to responders. Thus, together with the literature, our results suggest that the shape of three white matter bundles are associated to resistance severity and to the outcome of depression.

Second, our study focuses on two types of models: local and global shape analysis. Some local models seem to be sensitive to sampling effect, reflecting small variations in shape not captured by the global models. Finally, coherent global models imply coherent local models. To avoid false discoveries - and mainly because we artificially increased our dataset by adding noise to the bundles because of a too high number of covariates, hence reducing p-values - we had a conservative approach by asking the models to be coherent for local and global approaches. Note that for the bundles of interest: (CC7/OR/T-OCC) has for the global model a median p-value of (10e-11/10e-14/10e-18) and (10e-18/10e-

16/10e-13) for the local model (see supplementaries for more details). The study of bundles with coherent local models across samplings only (see Figure 2) is left for another study where we will have to investigate the optimal amount of noise to be added minimising the impact on statistics.

As literature validates our study on the outcome of depressed patients, in future work, we can study the association between those shape-based feature and the neurocognitive performance. Also, as it is suggested in a recent study [11] we will consider the entire fiber bundles segmentation as the shape, instead of there center lines.

6 Acknowledgment

This work was partly funded by Fondation de France, Rennes Metropole and defi scientifique from CNRS-Inserm. MRI data acquisition was supported by the Neurinfo MRI research facility from Rennes University. Neurinfo is granted by the European Union (FEDER), the French State, the Brittany Council, Rennes Metropole, Inria, Inserm and the Rennes University Hospital. This work has been funded by Institut des Neurosciences Cliniques de Rennes (INCR).

References

1. Batail, J.M., Coloigner, J., Soulas, M., Robert, G., Barillot, C., Drapier, D.: Structural abnormalities associated with poor outcome of a major depressive episode: The role of thalamus. Psychiatry Research: Neuroimaging **305** (2020)
2. Busner, J., Targum, S.D.: The clinical global impressions scale: applying a research tool in clinical practice. Psychiatry (Edgmont) **4**(7) (2007)
3. Cho, S.E., Park, C.A., Na, K.S., Chung, C., Ma, H.J., Kang, C.K., Kang, S.G.: Left-right asymmetric and smaller right habenula volume in major depressive disorder on high-resolution 7-T magnetic resonance imaging. PloS one **16**(8) (2021)
4. Coloigner, J., Batail, J.M., Commowick, O., Corouge, I., Robert, G., Barillot, C., Drapier, D.: White matter abnormalities in depression: A categorical and phenotypic diffusion MRI study. Neuroimage: clinical **22** (2019)
5. Commowick, O., Wiest-Daesslé, N., Prima, S.: Block-matching strategies for rigid registration of multimodal medical images. In: 2012 9th IEEE International Symposium on Biomedical Imaging (ISBI). IEEE (2012)
6. Coupe, P., Yger, P., Prima, S., Hellier, P., Kervrann, C., Barillot, C.: An Optimized Blockwise Nonlocal Means Denoising Filter for 3-D Magnetic Resonance Images. IEEE Transactions on Medical Imaging **27**(4), 425–441 (Apr 2008)
7. Cury, C., Glaunès, J.A., Colliot, O.: Diffeomorphic iterative centroid methods for template estimation on large datasets. In: Nielsen, F. (ed.) Geometric Theory of Information, pp. 273–299. Signals and Communication Technology, Springer International Publishing (2014)
8. de Diego-Adelino, J., Pires, P., Gomez-Anson, B., Serra-Blasco, M., et al.: Microstructural white-matter abnormalities associated with treatment resistance, severity and duration of illness in major depression. Psychological medicine (2014)
9. Garyfallidis, E., Brett, M., Correia, M.M., Williams, G.B., Nimmo-Smith, I.: Quickbundles, a method for tractography simplification. Frontiers in neuroscience **6** (2012)

10. GBD 2019, M.D.C., et al.: Global, regional, and national burden of 12 mental disorders in 204 countries and territories, 1990–2019: a systematic analysis for the global burden of disease study 2019. The Lancet Psychiatry (2022)
11. Glozman, T., Bruckert, L., Pestilli, F., Yecies, D.W., Guibas, L.J., Yeom, K.W.: Framework for shape analysis of white matter fiber bundles. NeuroImage (2018)
12. Gori, P., Colliot, O., Marrakchi-Kacem, L., Worbe, Y., De Vico Fallani, F., Chavez, M., Poupon, C., Hartmann, A., Ayache, N., Durrleman, S.: Parsimonious Approximation of Streamline Trajectories in White Matter Fiber Bundles. IEEE Transactions on Medical Imaging **35**(12) (Dec 2016)
13. Guy, W.: ECDEU assessment manual for psychopharmacology. US Department of Health, Education, and Welfare, Public Health Service, … (1976)
14. Hedouin, R., Commowick, O., Bannier, E., Scherrer, B., Taquet, M., Warfield, S.K., Barillot, C.: Block-Matching Distortion Correction of Echo-Planar Images With Opposite Phase Encoding Directions. IEEE Transactions on Medical Imaging **36**(5), 1106–1115 (May 2017)
15. Herrman, H., Patel, V., Kieling, C., Berk, M., Buchweitz, C., Cuijpers, P., Furukawa, T.A., Kessler, R.C., Kohrt, B.A., Maj, M., et al.: Time for united action on depression: a lancet–world psychiatric association commission. Lancet (2022)
16. Kennis, M., Gerritsen, L., van Dalen, M., Williams, A., Cuijpers, P., Bockting, C.: Prospective biomarkers of major depressive disorder: a systematic review and meta-analysis. Molecular psychiatry **25**(2) (2020)
17. Liao, Y., Huang, X., Wu, Q., Yang, C., Kuang, W., Du, M., Lui, S., et al.: Is depression a disconnection syndrome? meta-analysis of diffusion tensor imaging studies in patients with MDD. Journal of Psychiatry and Neuroscience **38** (2013)
18. Long, Y., Cao, H., Yan, C., Chen, X., Li, L., Castellanos, F.X., et al.: Altered resting-state dynamic functional brain networks in major depressive disorder: Findings from the REST-meta-MDD consortium. NeuroImage: Clinical **26** (2020)
19. Ourselin, S., Roche, A., Prima, S., Ayache, N.: Block matching: A general framework to improve robustness of rigid registration of medical images. In: International Conference on Medical Image Computing And Computer-Assisted Intervention. Springer (2000)
20. Pennec, X., Sommer, S., Fletcher, T.: Riemannian Geometric Statistics in Medical Image Analysis. Elsevier (2020)
21. Rush, A.J., Trivedi, M.H., Wisniewski, S.R., Nierenberg, A.A., Stewart, J.W., Warden, D., Niederehe, G., Thase, M.E., Lavori, P.W., Lebowitz, B.D., et al.: Acute and longer-term outcomes in depressed outpatients requiring one or several treatment steps: a star* d report. American Journal of Psychiatry **163**(11) (2006)
22. Schölkopf, B., Smola, A., Müller, K.R.: Nonlinear component analysis as a kernel eigenvalue problem. Neural Computation **10**(5), 1299–1319 (Jul 1998)
23. Serafini, G., Pompili, M., Borgwardt, S., Giuffra, E., Howes, O., Girardi, P., Amore, M.: The role of white matter abnormalities in treatment-resistant depression: a systematic review. Current pharmaceutical design **21**(10) (2015)
24. Tournier, J.D., Calamante, F., Connelly, A.: Robust determination of the fibre orientation distribution in diffusion MRI: non-negativity constrained super-resolved spherical deconvolution. Neuroimage **35**(4) (2007)
25. Tournier, J.D., Calamante, F., Connelly, A., et al.: Improved probabilistic streamlines tractography by 2nd order integration over fibre orientation distributions. In: Proceedings of the international society for magnetic resonance in medicine. vol. 1670. John Wiley & Sons, Inc. New Jersey, USA (2010)
26. Trouvé, A.: Diffeomorphisms groups and pattern matching in image analysis. International Journal of Computer Vision **28**(3), 213–221 (1998)

27. van Velzen, L.S., Kelly, S., Isaev, D., Aleman, A., Aftanas, L.I., et al.: White matter disturbances in major depressive disorder: a coordinated analysis across 20 international cohorts in the ENIGMA MDD working group. Molecular Psychiatry **25**(7), 1511–1525 (Jul 2020)
28. Wager, T.D., Woo, C.W.: Imaging biomarkers and biotypes for depression. Nature medicine **23**(1) (2017)
29. Wasserthal, J., Neher, P., Maier-Hein, K.H.: Tractseg-fast and accurate white matter tract segmentation. NeuroImage **183** (2018)
30. Yan, B., Xu, X., Liu, M., Zheng, K., Liu, J., Li, J., Wei, L., Zhang, B., Lu, H., Li, B.: Quantitative Identification of Major Depression Based on Resting-State Dynamic Functional Connectivity: A Machine Learning Approach. Frontiers in Neuroscience **14**, 191 (Mar 2020)